Modeling of a bubble column for CO$_2$ removal by absorption with NaOH

Michelson, Johan; Mäki-Arvela, Päivi; Rajala, Pasi; Hallapuro, Markus; Schmid, Daniel;
Karlström, Oskar; Wärnå, Johan; Murzin, Dmitry Yu

Document Version
Final published version

[Link to publication](#)

Modeling of a bubble column for CO$_2$ removal by absorption with NaOH

Johan Michelson, Päivi Mäki-Arvela, Pasi Rajala, Markus Hallapuro, Daniel Schmid, Oskar Karlström, Johan Wärnå & Dmitry Yu Murzin

Published online: 28 Sep 2023.

Submit your article to this journal ⬀

Article views: 432

View related articles ⬀

View Crossmark data ⬀

Modeling of a bubble column for CO_2 removal by absorption with NaOH

Johan Michelson[a], Päivi Mäki-Arvela[a], Pasi Rajala[b], Markus Hallapuro[b], Daniel Schmid[a], Oskar Karlström[a,c], Johan Wärnå[a], and Dmitry Yu Murzin[a]

[a]Johan Gadolin Process Chemistry Centre, Åbo Akademi University, Turku, Finland; [b]TM Systems Finland Oy, Turku, Finland; [c]Industrial Engineering and Management, Department of Mechanical and Materials Engineering, University of Turku, Turku, Finland

ABSTRACT

CO_2 capture experiments were carried out in a small-scale bubble column reactor using alkaline solutions of sodium hydroxide. The results of the experiments show that a higher NaOH content in the liquid phase and elevated CO_2 concentrations in the gas mixture led to a higher CO_2 removal efficiency. A mathematical model was developed to describe the CO_2 absorption as a function of CO_2 gas inlet and OH^- concentrations at low CO_2 and OH^- concentrations. The CO_2 uptake at high OH^- concentrations (high pH) was accurately predicted by the model, whereas the CO_2 uptake at lower OH^- concentrations could not be predicted with the same accuracy.

Introduction

Due to a substantial increase in the release of greenhouse gases (GHG) over the past century, more and more pressure has been put on manufacturing industries to minimize the amount of air pollutants released into the atmosphere. Carbon dioxide is the most critical GHG gas resulting from human activity. Other GHG gases are for example CH_4 and N_2O (Sanz-Perez et al. 2016). Therefore, intensive research efforts are focused on removing CO_2 emissions from industrial flue gases, in addition to the efforts of improving CO_2 removal in industrial processes (e.g. ammonia synthesis). The energy sector, which includes heat and electricity generation, transportation, manufacturing and construction, fugitive emissions, and other fuel combustion, is responsible for ca. 76% (37.2 Gt of carbon dioxide equivalents, CO_2e) of the total GHG emissions. For the rest, 11.9% (5.8 $GtCO_2e$) stems from agriculture, 5.9% (2.9 $GtCO_2e$) from direct industrial processes, such as ammonia synthesis mentioned above, 3.3% (1.6 $GtCO_2e$) reflects such waste as landfills and wastewater, while the remaining 2.8% (1.39 $GtCO_2e$) originates from land-use change and forestry.

Flue gases from a range of industrial processes contain 8–14 vol-% CO_2. Production of aluminum generates CO_2 effluent with 4% concentration (Lorentsen et al. 2016).

The net GHG emissions from the pulp and paper industry release only 0.8% of all worldwide GHG emissions, i.e., 0.39 $GtCO_2e$ (Mengpin et al. 2020), with the paper production being the main contributor to such release in particular the drying section of paper machines. A particular feature of the paper industry is a low content of CO_2 in the effluent gas, which is emitted at atmosperic pressure. This restrictions make removal of carbon dioxide from such effluents very challenging.

It is well known that physical adsorption of CO_2 is a potential method for reducing CO_2 emissions (Belmabkhout et al. 2016), however, the drawback is a high price of the adsorbents. Several conventional methods for CO_2 removal such as absorption, have usually been investigated with sodium hydroxide (NaOH), monoethanolamine (MEA) or other amines, such as methyldiethanolamine (MDEA) (Luis 2016). A major difference between MEA and NaOH is that MEA can be readily regenerated, while during CO_2 absorption with NaOH; $NaHCO_3$ and finally

Na_2CO_3 are formed, where the latter one is thermally stable (Heda et al. 1995; Siriwardane et al. 2007).

When using NaOH as an absorbent typically pure CO_2 (Darmana et al. 2007) or a mixture containing a relatively high fraction of CO_2 (20%) (Zhang et al. 2007) or 30% (Yoo et al. 2013) have been used. The latter feedstock with 30% CO_2 represents cement and steel industries effluent. For such cases CO_2 capture efficiency was reported to increase with increasing NaOH concentrations, giving first order kinetics for formation of Na_2CO_3 from NaOH and CO_2 when sodium hydroxide concentration was varied in the range of 1–5 wt.% (Yoo et al. 2013).

CO_2 removal from atmospheric air with a strong hydroxide solution has been demonstrated by Keith et al. (2018) with 1 M [OH^-]. However, according to the knowledge of the authors, removal of CO_2 by absorption with a very low CO_2 concentration from effluent gases and low concentration of OH^- in the scrubbing liquids has not been properly addressed in scientific literature.

In the current work the main aim is to study CO_2 absorption in aqueous sodium hydroxide using a laboratory scale bubble column. The bubble columns are often used in industry for industrial processes per se as well as for investigation of carbon dioxide removal from various effluences (Papari et al. 2014; Khadem-Hamedani et al. 2015; Chen and Zhuo 2020; Inkeri and Tynjälä 2020; Salmi et al. 2023). Different models for the columns are often used exploring the impact of the flow regimes and the effect of mass transfer on the chemical reactions or absorption of gases.

The main parameters investigated in the current work are CO_2 concentration in the range $1000 - 20\ 000$ ppm and pH of the absorbent, which was between 8 and 14.

The conditions of the experiments correspond to emissions of the industries when the concentration of carbon dioxide is rather low, as for example in emissions from paper machines.

Experimental

The CO_2 absorption experiments were performed in a bubble column system, into which the gas was fed through a sintered glass filter from the bottom of the column through the scrubbing liquid. The experiments were performed at room temperature. The CO_2 absorption efficiency was investigated at different pH by preparing 50 ml NaOH solution at pH 14, 13, and 12. A carbonate buffer of 0.1 M was used for pH 10 and 0.1 M of the phosphate buffer at pH 8 was applied due to very fast reaction times and rapid NaOH consumption in the laboratory tests. Utilization of the buffers, which role was to maintain the pH of the scrubbing liquid, does not change the rate of absorption, because the latter is determined by the number of hydroxide ions (OH^-) reacting with CO_2 in the alkaline solution.

A continuous gas analyzer Servomex 4900 was used to measure the CO_2 content of the outflowing gas and the flow balances were calculated from the gathered data. The gas analyzer was coupled to a programmable data logger OM-CP-OCTPRO by Omega, which saves the measured data in logs on a USB drive. The inlet gas mixture was composed of a mixture of nitrogen, CO_2, and argon, where N_2 (Woikoski, 99%) and Ar act as inert gases. The gas bottle of CO_2 was composed of 2% CO_2 and 98% Ar. By using a diluted CO_2 gas mixture, it is possible to use a feed gas containing 1000 ppm CO_2. The gas inlet flows were controlled by a flow controller Bronkhorst, F-201C-RAA-33-E, to change the CO_2 feed gas concentration. Repeated tests showed nearly identical measurement signals, and therefore the experiments were only repeated twice. A mean value for these pairs of experiments was calculated to find the median for the CO_2 absorption efficiency of NaOH solutions at different pH with varying CO_2 gas concentrations.

The bubble column was a glass bottle with a diameter of 5 cm, which was filled with 50 mL of the absorption liquid. The incoming gas entered the liquid through a porous glass sinter with a diameter of 2 cm to ensure small bubble sizes. The height of the liquid above the sinter was 15 mm. The gas flow rate was 2 l/min.

The gas bubble sizes in the bubble column were recorded using a high-speed camera Photron SA3 and software ImageJ was applied for image processing and bubble size measurements. The generated results were statistically analyzed thereafter

and processed using the Origin software. The bubble rising velocity was measured with the Photron fastcam viewer software.

Theory

Reaction mechanism

When a strong alkaline compound such as NaOH is in contact with pure water, the alkaline compound is completely ionized. In this case, NaOH is dissociated into sodium cations (Na^+) and hydroxide anions (OH^-). At pH > 10, hydroxylation is the dominant reaction where CO_2 absorption is controlled by reactions (1) and (2) (Kern 1960).

$$CO_2(aq) + OH^-(aq) \rightleftharpoons HCO_3^-(aq) \qquad (1)$$

$$HCO_3^- + OH^-(aq) \rightleftharpoons CO_3^{2-} + H_2O(l) \qquad (2)$$
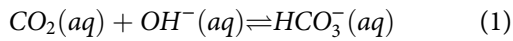
At high pH when equilibrium is shifted to the right side of Equations (1) and (2), they may be combined giving the following irreversible reaction:

$$CO_2(aq) + 2OH^-(aq) \rightarrow CO_3^-(aq) + H_2O(l) \qquad (3)$$
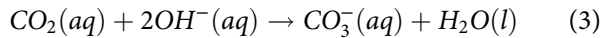
However, when pH < 10, hydration plays an important part when absorbing CO_2 and dominant when pH < 8. Hydration consists of two reactions: CO_2 combines first with water to produce carbonic acid, which then reacts with OH^- resulting in bicarbonate and water (Kern 1960):

$$CO_2(aq) + H_2O(l) \rightleftharpoons H_2CO_3(aq) \qquad (4)$$

$$H_2CO_3(aq) + OH^-(aq) \rightleftharpoons HCO_3^- + H_2O(l) \qquad (5)$$
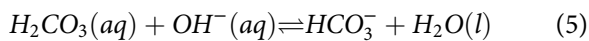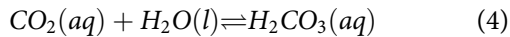
Definitions

The absorption efficiency η of CO_2 in NaOH solutions can be estimated using:

$$\eta = \left(1 - \frac{C_{CO2,out}}{C_{CO2,in}}\right) \times 100 \qquad (6)$$

In addition, the mean absorption efficiency of both experimental repetitions was calculated from:

$$\eta_{mean} = \frac{\eta_{rep1} + \eta_{rep2}}{2} \qquad (7)$$

The amount of absorbed CO_2 in the alkaline solution is determined from:

$$r_{diss,CO2} = C_{CO2,in} - C_{CO2,out}, \qquad (8)$$

where the amount of $r_{diss,CO2}$ and the concentration of CO_2 in the gas inlet and outlet are given in ppm.

The rate of absorption R_A (mol/min) is the amount of CO_2 chemically absorbed by the NaOH solution defined by

$$R_A = Q_g \ (C_{CO2,in} - C_{CO2,out}), \qquad (9)$$

where Q_g is the gas flow rate (L/min) and C is the concentration (mol/L) of the CO_2 in the inlet and outlet gas. The absorption rate depends on the mass transfer coefficient k_L (m/s), interfacial area a (m^2/m^3) and the enhancement factor E. Equation (9) can therefore be expanded to the following equation (Wongwailikhit 2019):

$$Q_g \ (C_{CO2,in} - C_{CO2,out}) = E \ k_L a \ \Delta C_{ln,mean} V_{total} \qquad (10)$$

The interfacial area between the liquid and the gas phases, is defined as the total interfacial area per unit volume of the contactor. When assuming spherical bubbles, the interfacial area for the bubble column can be calculated according to Wongwailikhit (2019)

$$a = \frac{6}{d_{32}} \ \frac{\varepsilon_g}{1 - \varepsilon_g}, \qquad (11)$$

where, d_{32} (mm) represents the Sauter mean diameter and ε_g (%) corresponds to the gas holdup in the column. The Sauter mean diameter, the diameter of a sphere that has the same volume-to-surface area ratio as the measured bubbles, which usually are in the form of an ellipse, is calculated as:

$$d_{32} = \frac{\sum_i n_i d_i^3}{\sum_i n_i d_i^2}, \qquad (12)$$

where n_i is the number of bubbles having a diameter of d_i (Maceiras et al. 2010). A 500 fps film was recorded with a high-speed camera to determine d_{32}. In particular, 15–20 bubbles were measured from 50 randomly chosen frames of the recorded film. Only bubbles below a specific height were measured as the actual sample volume used in the absorption experiments was 50 ml, whereas a volume of 100 ml was used for the film capture.

The gas holdup, ε_g, which represents the gas fraction present in the gas-liquid system, is defined as:

$$\varepsilon_g = \frac{V_g}{V_g + V_L} \qquad (13)$$

where V_g and V_L are the gas and liquid volumes in the system, respectively.

The gas holdup can also be calculated as:

$$\varepsilon_g = \frac{Q_g}{u_b A_c} = \frac{U_g}{u_b} \tag{14}$$

where u_b is the bubble rising velocity, A_c is the cross-sectional area of the bubble column and U_g is the superficial gas velocity.

The overall mass transfer coefficient K_L is the rate of mass transfer between the bulk solution and the saturated film. The equilibrium relationship between the overall mass transfer coefficient and the individual mass transfer coefficients is given by Equation (15), where H_A is the Henry's constant, k_L is the liquid side mass transfer coefficient and k_G is the gas side mass transfer coefficient (Salmi et al. 2023).

$$\frac{1}{K_L} = \frac{1}{k_L A_c} + \frac{1}{H_A k_G} \tag{15}$$

For poorly soluble gases, e.g. CO_2, the mass transfer is limited at the liquid phase. Thus, the overall mass transfer coefficient is approximately the same as the liquid side mass transfer coefficient, $K_L \approx k_L$.

The liquid side mass transfer coefficient k_L was calculated according to the Higbiés penetration theory, Equation (16), which assumes both an unsteady state of mass transfer during the contact time t_c and equilibrium at the gas-liquid interface (Wongwailikhit 2019). The reason for using the Higbiés penetration theory is that many industrial mass transfer processes have a contact time between the phases not sufficient to achieve a steady state, thus the film theory, not accounting for such non-stationarity, cannot be applied

$$k_L = 2\sqrt{\frac{D_{CO2}}{\pi \, t_c}} \tag{16}$$

$$t_c = \frac{d_{32}}{u_b} \tag{17}$$

where D_{CO2} is the diffusion coefficient for CO_2 in water, equal to $1.91 \times 10^{-9} \frac{m^2}{s}$ (Engineering ToolBox 2008). The limitations of the Higbie approach are well known, as the penetration theory should be applied for high Reynolds numbers

and the values of k_L are diminishing with a decrease in bubble rise velocity.

The enhancement factor E is used to estimate the enhanced effect of chemical absorption compared to physical absorption alone. The enhancement factor for physical absorption is thus equal to unity, while the enhancement factor for chemical absorption is $E > 1$. To estimate E, both the Hatta number M_H and the enhancement parameter E_i must be determined through the equations below (Levenspiel 1999).

$$M_H = \sqrt{\frac{k_r C_{OH} D_{CO2}}{k_L^2}} \tag{18}$$

$$E_{AL} = E_i = 1 + \frac{D_{OH} C_{OH} H_A}{b D_{CO2} p_{CO2}} \tag{19}$$

The Hatta number is calculated through Equation (18), where k_r is the reaction constant for the second order reaction of CO_2 and OH^-. In this work, a value of $5157.43 \frac{L}{mol \, s}$ at $18\,°C$ is used for k_r which is the second order reaction rate constant of CO_2 reacting with OH^- (Wongwailikhit 2019).

As presented in Equation (19), the enhancement parameter E_i depends on both the OH^- concentration and the CO_2 partial pressure, where b is the stoichiometric constant for OH^- in the reaction being equal to 2, and D_{OH} is the diffusion coefficient for OH^- in water, which is $5.27 \times 10^{-9} \frac{m^2}{s}$ (Aqion 2020). A graphical method can be used to estimate the enhancement factor E when both M_H and E_i are known (Levenspiel 1999). The reaction can be considered an intermediate case if M_H is between 0.02 and 2, and the enhancement factor can be calculated according to $E \cong 1 + M_H^2/3$.

The reaction order is here determined using the following logarithmic equation

$$ln\left(\frac{-dc_A}{dt}\right) = ln\,k + n\,ln\,c_A, \tag{20}$$

where the slope n corresponds to the reaction order.

The absorption efficiency was estimated from the amount dissolved CO_2 from the gas phase, which can be converted into absorption efficiency according to:

$$\eta = \frac{\Gamma_{diss,\,CO2}}{C_{CO2,\,in}}. \tag{21}$$

Results and discussion

CO$_2$ absorption efficiency at different pH and CO$_2$ gas concentrations

The data from the CO$_2$ absorption experiments show the inlet and outlet CO$_2$ concentrations as a function of time from the experimental bubble column (Figure 1). A steep decline in CO$_2$ concentration is visible, followed by a small rise, which subsequently levels off can be seen in the figure. The steep decline is the point in time when the feed gas is allowed to flow through the column as the bypass is shut. As some air is left inside the column due to the bubble column being operated in a batch mode, a small rise of CO$_2$ concentration from the lowest point can be noticed. The point where the CO$_2$ concentration is relatively constant was taken as a measure for CO$_2$ removal efficiency of respective pH.

The mean CO$_2$ removal efficiency of NaOH at pH 8, 10, 12, and 14 at CO$_2$ gas concentrations of 1000, 2500, 5000, 10000 and 20000 ppm, respectively is shown in Figure 2 and Table 1. The highest absorption efficiency was achieved at pH 14, whereas the lowest absorption efficiency was obtained at pH 8. These results are clearly linked to the amount of OH$^-$ in the solution reacting with the aqueous CO$_2$, as pH 14 corresponds to 10-fold more hydroxide ions than pH 13 and one million times more than pH 8.

The error margin estimated from the standard deviation based accuracy of the analyzer,
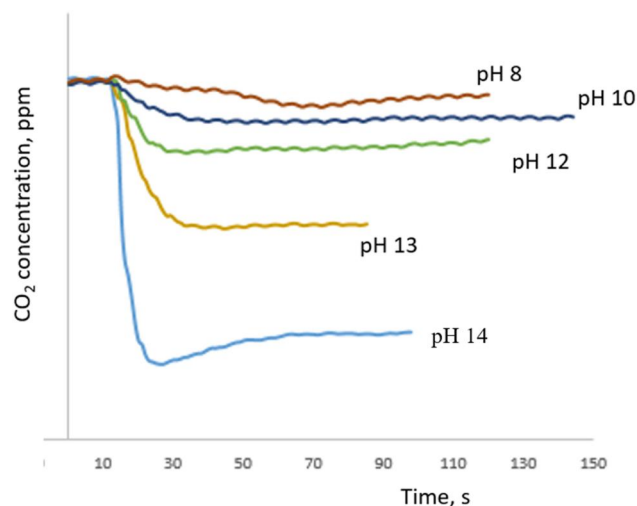
250 ppm, is also included in the figure, which shows how the accuracy of the analyses drastically decreases with decreasing CO$_2$ concentrations. For CO$_2$ concentrations above 20000 ppm, an error margin of less than 3% was obtained. However, for lower CO$_2$ concentrations, such as 5000 ppm, the error margin is 10%, whereas for 2500 ppm and 1000 ppm, the error margin is increasing substantially to 25% and 50%, respectively. Although the margin of error is quite large, a clear trend can be seen in Figure 2, showing how the CO$_2$ absorption efficiency increases with decreasing CO$_2$ concentrations in the feed gas and higher pH of the scrubbing liquid. Judging from absorption efficiency *per se* in the studied range of parameter the optimal pH for absorbing CO$_2$ is clearly 14, whereas the least optimal is pH 8. This trend is well known and has been noted by Kordylewski et al. (2013; Yoo et al. 2013), who found that increasing NaOH concentration also increases CO$_2$ capture efficiency. Kordylewski et al. (2013) also found that increasing temperature intensifies CO$_2$ absorption by accelerating the reaction in the solution thus increasing CO$_2$ absorption efficiency.

The influence of the CO$_2$ gas concentration on the CO$_2$ absorption efficiency has not been widely studied. A fine spray scrubber was used by Zhenqi et al. (2009) to study this effect where the CO$_2$ gas concentration was varied between 7 and 15% (v/v) in a spray of NaOH solution at

Figure 1. Measured CO$_2$ gas concentration after the bubble column scrubber as a function of time.
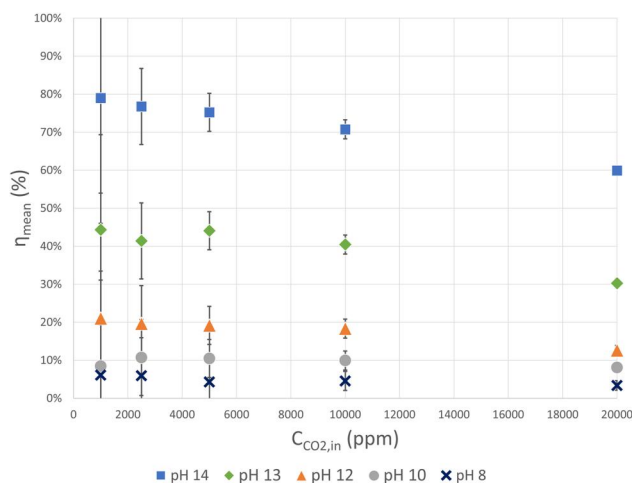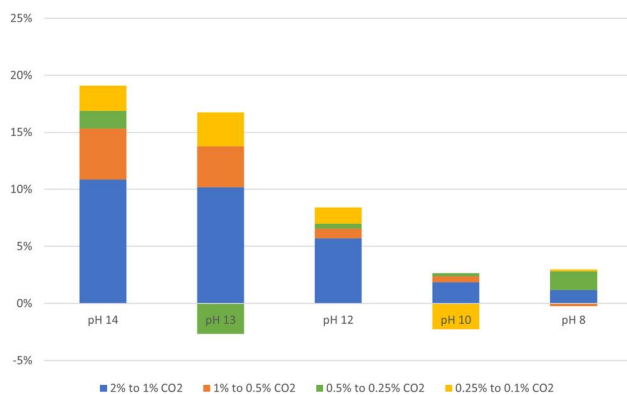

Figure 2. Mean CO$_2$ removal efficiency of alkaline solutions at different pH and CO$_2$ gas inlet concentrations, including error margins estimated from standard deviation based accuracy of the gas analyzer.

Table 1. Mean CO_2 absorption efficiency of two repetitions of experiments.

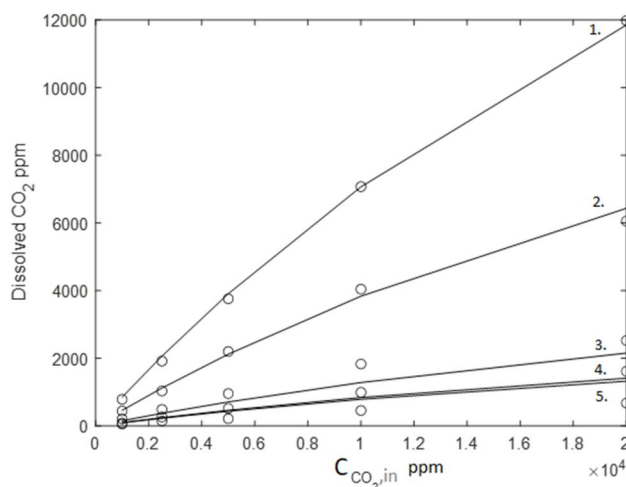| $C_{CO2,in}$ [ppm]	η_{mean} [%] pH 14	η_{mean} [%] pH 13	η_{mean} [%] pH 12	η_{mean} [%] pH 10	η_{mean} [%] pH 8
20000	63	31	12	8	3
10000	71	41	18	10	5
5000	78	44	19	9	3
2500	76	42	19	10	6
1000	78	48	20	8	5

Figure 3. Difference in absorption efficiency of carbon dioxide at different CO_2 concentrations as a function of pH.

Figure 4. Mathematical model fit of dissolved CO_2 compared to the experimental data, where the dots correspond to the data points and the lines represent the calculations. The inlet CO_2 concentrations of the gas are denoted as follows: 1. 20000 ppm, 2. 10000 ppm, 3. 5000 ppm, 4. 2500 ppm, 5. 1000 ppm. Points represent the experimental data, while lines are the model fit.

5% (w/w). The results of Zhenqi et al. (2009) showed a slight decrease in CO_2 absorption efficiency with increased CO_2 gas concentration. The results of this work seem to confirm this behavior also at lower CO_2 concentrations in the gas mixture.

The cumulative difference in absorption efficiency between CO_2 gas concentrations at each pH shown in Figure 3 illustrates its decrease with decreasing pH. However, the difference in absorption efficiency can be seen to both increase and decrease for CO_2 gas concentrations of 0.5–0.25% and 0.25–0.1% CO_2, which can be explained by the low accuracy of the gas analyzer at low CO_2 concentrations.

The amount of dissolved CO_2 decreased with decreasing inlet CO_2 concentration as illustrated in Figure 4 with the corresponding logarithmic plots of the absorption isotherms (Equation (22)) presented in Figure 5.

The reaction order toward [OH⁻] was calculated giving a value equal to ca. 0.2. The absorption isotherms are shown to be nonlinear and of higher order at high pH. The fractional reaction order indicates that the reaction is of a complex mechanism, which is plausible, as the absorption of CO_2 in NaOH occurs in a two-step reaction.

Modeling the amount of dissolved CO_2

The amount of CO_2 absorbed as a function of CO_2 concentration of the feed gas and concentration of OH⁻ in the scrubbing liquid is depicted in Figure 4. In the figure, the amount of absorbed CO_2 rapidly increases at low gas partial pressures and consequently levels off at high gas partial pressures, as the absorbate approaches saturation. This behavior seems to resemble the Langmuir adsorption isotherm (Privalova et al. 2013), where the maximum adsorption capacity corresponds to a monosaturated layer of adsorbate molecules on the surface of an adsorbent. Based on the study done by Karbalaei Mohammad et al. (2020), the behavior also resembles the Sips adsorption isotherm, which is a combination of the Langmuir and the Freundlich model, where the Freundlich model takes into account the heterogeneous surface of the adsorbate (Abin-Bazaine et al. 2022).
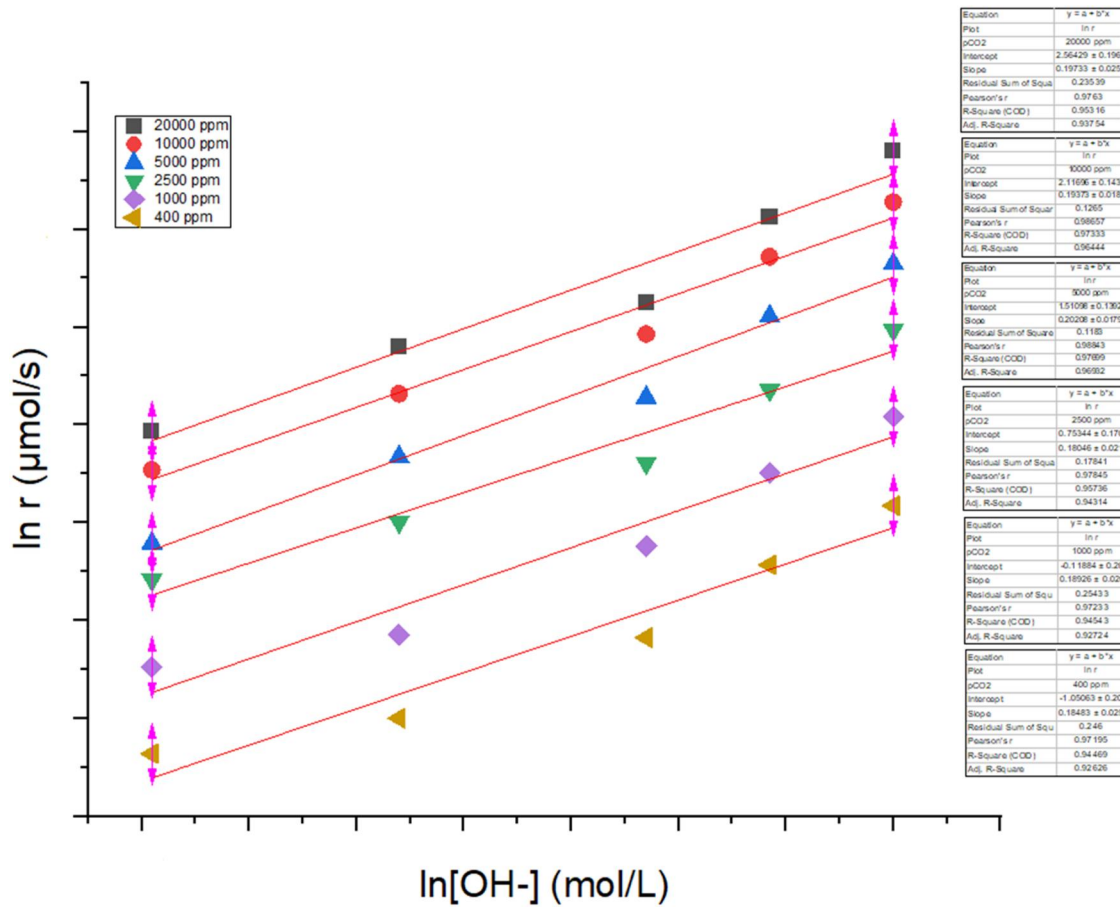
Figure 5. Logarithmic plot of the experimental data, showing dependence of the logarithm of the rate vs OH^- concentration.

In Equation (22), the amount of dissolved CO_2, $r_{diss, CO2}$ (ppm), in alkaline solutions is shown to be dependent on both the concentration of CO_2 in the gas phase as well as the $[OH^-]$ concentration in the liquid phase. In addition, both reactants may function as the limiting ones in the chemical reaction. Thus, $r_{diss, CO2}$ as a function of $[OH^-]$ and CO_2 inlet gas concentration at low $[OH^-]$ concentrations can be estimated through the developed semi-empirical mathematical model:

$$r_{diss, CO2} = \frac{k\ C_{CO2}}{1 + k_3 C_{CO2}}\ \frac{k_4 + k_1[OH^-] + k_2[OH^-]^2}{1 + k_1[OH^-] + k_2[OH^-]^2},$$

$$(22)$$

where the left part of the equation describes the effect of CO_2 concentration in the gas and the saturation behavior of the liquid on the amount of absorbed CO_2. The right-side fraction describes the effect of the $[OH^-]$ concentration of the two-step reaction mechanism of CO_2 and NaOH.

At high OH^- concentrations, the model fits the experimental data reasonably well, while some slight deviations can be seen for low pH values (lower $[OH^-]$ concentration in Figure 5), namely underestimating CO_2 uptake at pH 8 for the inlet concentration of 400–2500 ppm and overestimating at pH 10 for the inlet carbon dioxide concentration of 400–1000 ppm, which can be also related to the data precision. Overall, the model fits the experimental data fairly well and can be used to estimate the CO_2 uptake as a function of the CO_2 gas concentration of the feed gas and the OH^- concentration of the scrubbing liquid (Figure 6). The parameter values alongside their standard errors are shown in Table 2, displaying relatively small errors. The interfacial area and mass transfer coefficient, on the other hand, are distinct parameters for each CO_2 scrubbing contactor. Hence, when applying the mathematical model, a correction factor for the overall mass transfer coefficient in comparison to the experimental column utilized in this work should be taken into consideration.

Determination of the Hatta number and the enhancement factor

Figure 7a illustrates a captured frame with the high-speed camera and Figure 7b shows a processed image with ImageJ, from where the bubbles can be more distinguishable from one another. As can be seen from Figure 7 there is apparently

Table 2. Parameter values with the standard errors of the mathematical model.

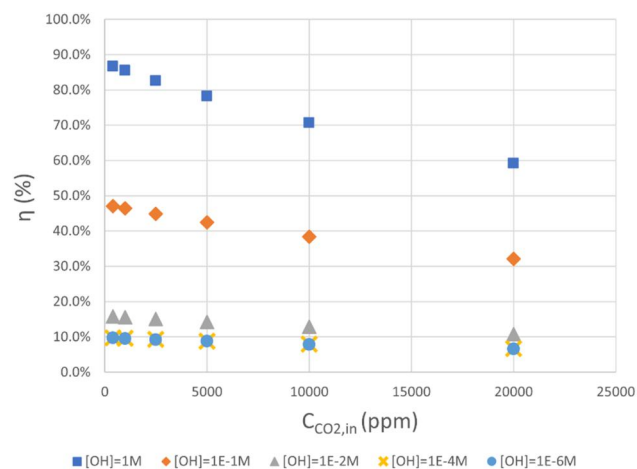| Parameters	Units	Parameter value	Std. Error (%)
k	ppm^{-1}	0.979	5.7
k1	L/mol	0.749×10^{1}	10.3
k2	L^{2}/mol^{2}	0	0
k3	ppm^{-2}	0.239×10^{-4}	18.9
k4	–	0.1	0

Figure 6. The predicted CO_2 absorption efficiency as a function of CO_2 gas inlet concentration and OH^- concentration.

no substantial bubble size distribution in the radial direction. The bubble size distribution was determined in the column in the axial direction to calculate the Sauter mean diameter. The bubble size distributions across the column, from the gas exit to the 27 cm mark on the ruler (Figure 7), are shown in Figures 8 and 9 for two hundred and one thousand bubbles displaying the average measured bubble diameter of ca. 1.4 mm for both cases despite some visual differences in the distribution. Furthermore, the Sauter mean diameter of 2 mm was derived from Equation (12).

Some calculated parameters of the bubble column used in this work with a gas flow rate of 2 L/min, and the superficial gas velocity of 0.017 m/s are shown in Table 3.

The bubble rising velocity was measured and the gas holdup was calculated according to Equation (14). The derived value for the gas holdup seems to be in good agreement with the experimental work of Krishna and Van Baten (2003), who determined the correlation between the superficial gas velocity and the gas holdup in a bubble column with a diameter of 10 cm. Based on that study the bubble flow in the bubble column of the current work is in the transition regime between the homogeneous and heterogenous regimes. During absorption the bubble coalescence occurs because of collisions and break-up of the bubbles. The bubble sizes also change due to the interfacial mass transfer when
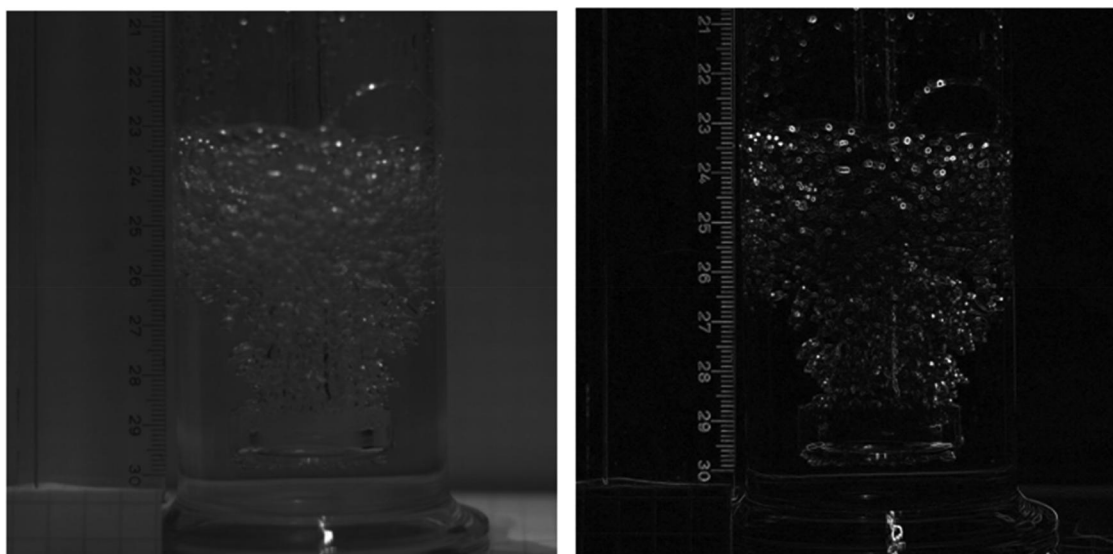

Figure 7. Captured images a) with Photron SA3 b) processed image with ImageJ.

a gas is dissolved (Gruber et al. 2015). The bubble coalescence was difficult to be observed in the current work, as the bubble flow is not fully in the heterogeneous regime.
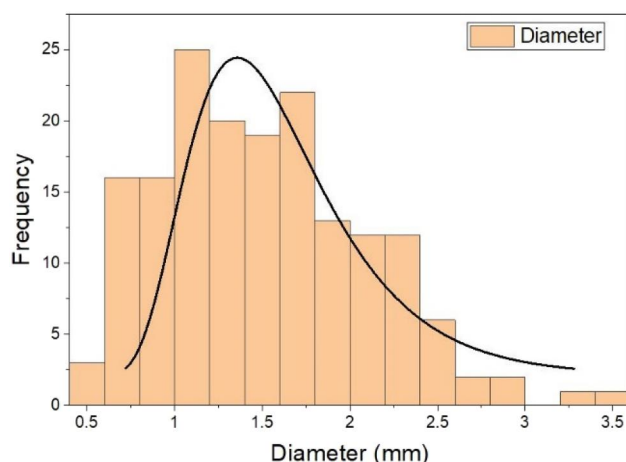

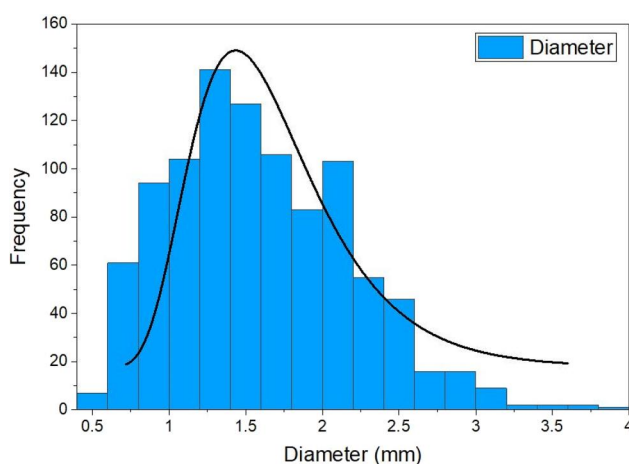**Figure 8.** Bubble size distribution based on ca. 200 bubbles.

Figure 9. Bubble size distribution based on ca. 1000 bubbles.

Table 3. Calculated values for the parameters based on the experiments in a bubble column.

Parameter	Value	Units
Q_g	2	L/min
d_C	5	cm
U_g	0.017	m/s
d_{32}	2	mm
a	203	m^2/m^3

The bubble column's interfacial area was calculated to be $203 \, m^2/m^3$, which is in the middle of the range of typical values for bubble columns, usually varying from 50 to $400 \, m^2/m^3$. The liquid side mass transfer coefficient k_L of the experimental bubble column appears to be in the higher range of typical values ($1 - 5 \times 10^{-4}$ m/s) for bubble columns (Salmi et al. 2023). The same was valid for the overall mass transfer coefficient of the bubble column. Seemingly, the high mass transfer appears to be a result of the experimental bubble column small bubble sizes and a low gas flow rate.

The calculated Hatta number M_H, the enhancement parameter E_i and the enhancement factor E for the reactions studied in the current work are shown in Tables 4 and 5. The enhancement factor of pH 14 was calculated to be 5.5, while for pH 13 it was ca. 2. For pH $\leq$ 13, the enhancement factor was close to 1. The enhancement factor showed almost no dependence on CO_2 gas concentrations. The calculated results for the Hatta number and enhancement factor demonstrated that for pH 14, i.e., $1 \, M \, OH^-$, the reaction is of pseudo-first order. This seems to agree also with the previous work (Stolaroff et al. 2008), stating that CO_2 reacting with NaOH is of pseudo-first order at OH^- concentrations above $1 \, M$.

The magnitude of the Hatta number can be used to assess the reaction phase. When the pH of the alkaline solution is less than 14 but higher than 8, the reactions are in the intermediate regime as $0.02 < M_H < 2$, meaning that the reaction occurs partly within the bulk liquid and

Table 5. The Hatta number M_H (Equations (18)) and the enhancement factor E^* at different pH.

Parameter	pH 14	pH 13	pH 12	pH 10	pH 8
M_H	5.54	1.75	0.55	0.06	0.01
E	5.54	2.02	1.10	1.00	1.00

*Determined using the graphical method (Wongwailikhit 2019).

Table 4. The enhancement parameter as a function of CO_2 gas concentrations and pH.

Enhancement parameter E_i					
$C_{CO2, in}$ [ppm]	pH 14	pH 13	pH 12	pH 10	pH 8
20000	1.98×10^3	1.98×10^2	2.07×10^1	1.04×10^0	1.00×10^0
10000	3.95×10^3	3.96×10^2	3.96×10^1	1.20×10^0	1.00×10^0
5000	7.9×10^3	7.91×10^2	8.00×10^1	1.39×10^0	1.01×10^0
2500	1.58×10^4	1.58×10^3	1.59×10^2	2.58×10^0	1.02×10^0
1000	3.95×10^4	3.95×10^3	3.96×10^2	4.95×10^0	1.04×10^0

partly within the liquid film. According to Levenspiel (1999) for $M_H < 0.02$ the reaction occurs only in the bulk liquid, whereas for $M_H > 2$ the reaction takes place only in the liquid film. From Table 5, it can be concluded that in the current case the reaction occurs only in the liquid film at pH 14, below pH 14 it proceeded in both the liquid film and the bulk of the liquid. Finally, at pH 8 the reaction is infinitely slow and the liquid bulk volume is the controlling rate factor.

Conclusions

While CO_2 capture has been a subject of extensive research and enormous practical experience has been accumulated along the years, removal of CO_2 by absorption with a very low CO_2 concentration from effluent gases and low concentration of OH^- in the scrubbing liquids has not been investigated. The current study fills this void by investigating CO_2 absorption in aqueous sodium hydroxide using a laboratory scale bubble column varying the CO_2 concentration in the range $1000 - 20\ 000$ ppm and pH of the absorbent between 8 and 14.

Higher NaOH content in the liquid phase and elevated CO_2 concentrations in the gas mixture led to a higher CO_2 removal efficiency with a fractional order toward $[OH^-]$ equal to 0.2 and the highest efficiency was achieved at pH 14. The shapes of absorption isotherms regarding CO_2 concentrations resemble the Langmuir isotherm.

A mathematical model valid at least in the studied CO_2 concentration and pH ranges was developed to describe the CO_2 absorption as a function of CO_2 gas inlet and OH^- concentrations at low CO_2 and OH^- concentrations. The CO_2 uptake at high OH^- concentrations was accurately predicted by the model, whereas the CO_2 uptake at lower OH^- concentrations was slightly over- and underestimated.

The bubble size distribution was determined to calculate the Sauter mean diameter in the column operating in the transition between the homogeneous and heterogeneous regimes. The experimentally measured value of ca. 1.4 mm was close to the theoretical one equal to ca. 2 mm. The calculated results for the Hatta number and the enhancement factor demonstrated that for pH 14,

i.e., 1 M OH^-, the reaction is of pseudo-first order. At pH 14 the reaction occurs only in the liquid film, while below 14 it proceeded also in the bulk of the liquid.

Note that the Hatta number, enhancement factor and even absorption efficiency cannot serve as the sole descriptors to determine the optimal conditions for carbon dioxide removal in an industrial process. While pH 14 might look preferential from the viewpoint of efficiency, there are also many factors, including process economics, corrosion, etc, determining the optimal conditions. This would require subsequently a proper techno-economic analysis.

Disclosure statement

References

Abin-Bazaine A, Trujillo AC, Olmos-Marquez M. 2022. Adsorption isotherms: enlightenment of the phenomenon of adsorption. In: Muharrem Ince, Olcay Kaplan Ince editors, Wastewater treatment. Rijeka: IntechOpen. p. 3–7. doi:10.5772/intechopen.104260.

Aqion. 2020. Table of diffusion coefficients. [accessed 2022 Feb 21]. https://www.aqion.de/site/diffusion-coefficients.

Belmabkhout Y, Guillerm V, Eddaoudi M. 2016. Low concentration CO2 capture using physical adsorbents: are metal–organic frameworks becoming the new benchmark materials? Chem Eng J. 296:386–397. doi:10.1016/j.cej.2016.03.124.

Chen PC, Zhuo SH. 2020. CO_2 capture in a bubble-column scrubber using MEA/CaCl$_2$/H$_2$O solution-absorption and precipitation. Crystals. 10:694. doi:10.3390/cryst10080694.

Darmana D, Henket RLB, Deen NG, Kuipers JAM. 2007. Detailed modelling of hydrodynamics, mass transfer and chemical reactions in a bubble column using a discrete bubble model: chemisorption of CO_2 into NaOH solution, numerical and experimental study. Chem Eng Sci. 62:2556–2575. doi:10.1016/j.ces.2007.01.065.

Engineering ToolBox. 2008. https://www.engineeringtoolbox.com/.

Gruber MC, Radl S, Khinast JG. 2015. Rigorous modeling of CO_2 absorption and chemisorption. The influence of bubble coalescence and breakage. Chem Eng Sci. 137:188–204. doi:10.1016/j.ces.2015.06.008.

Heda PK, Dollimore D, Alexander KS, Chen D, Law E, Bicknell P. 1995. A method of assessing solid state reactivity illustrated by thermal decomposition experiments on sodium bicarbonate. Thermochim Acta. 255:255–272. doi:10.1016/0040-6031(94)02154-G.

Inkeri E, Tynjälä T. 2020. Modelling of CO_2 capture with water bubble column reactor. Energies. 13:5793. doi:10.3390/en13215793.

Karbalaei Mohammad N, Ghaemi A, Tahvildari K, Sharif AAM. 2020. Experimental investigation and modeling of CO_2 adsorption using modified activated carbon. Iran J Chem Chem Eng. 39:177–192.

Keith DW, Holmes G, Angelo DS, Heidel K. 2018. A process for capturing CO_2 from the atmosphere. Joule. 2:1573–1594. doi:10.1016/j.joule.2018.05.006.

Kern DM. 1960. The hydration of carbon dioxide. J Chem Educ. 37:14–23. doi:10.1021/ed037p14.

Khadem-Hamedani B, Yaghmaei S, Fattahi M, Mashayekhan S, Hosseini-Ardali SM. 2015. Mathematical modelling of a slurry bubble column for hydrodesulfurization of diesel fuel: single- and two-bubble configurations. Chem Eng Res Des. 100:362–376. doi:10.1016/j.cherd.2015.05.023.

Kordylewski W, Sawicka D, Falkowski T. 2013. Laboratory tests on the efficiency of carbon dioxide capture from gases in NaOH solutions. J Ecol Eng. 14:54–62. doi:10.5604/2081139X.1043185.

Krishna R, Van Baten JM. 2003. Mass transfer in bubble columns. Catal Today. 79:67–75. doi:10.1016/S0920-5861(03)00046-4.

Levenspiel O. 1999. Chemical reaction engineering. New York: John Wiley & Sons.

Lorentsen O-A, Dyroy A, Karlsen M. 2016. Handling CO2EQfrom an aluminum electrolysis cell. In: Bearne G, Dupuis M, Tarcy G, editors. Essential readings in light metals. Switzerland: Springer International Publishers. p. 975–980.

Luis P. 2016. Use of monoethanolamine (MEA) for CO_2 capture in a global scenario: consequences and alternatives. Desalination. 380:93–99. doi:10.1016/j.desal.2015.08.004.

Maceiras R, Álvarez E, Cancela M. 2010. Experimental interfacial area measurements in a bubble column. Chem Eng J. 163:331–336. doi:10.1016/j.cej.2010.08.011.

Mengpin G, Friedrich J, Vigna L. 2020. 4 charts explain greenhouse gas emissions by countries and sectors. Washington (DC): World Resource Institute.

Papari S, Kazameini M, Fattahi M, Fatahi M. 2014. DME direct synthesis from syngas in a large-scale three-phase slurry bubble column: transient modeling. Chem Eng Commun. 201:612–634. doi:10.1080/00986445.2013.782292.

Privalova E, Rasi S, Mäki-Arvela P, Eränen K, Rintala J, Murzin DY, Mikkola JP. 2013. CO2 capture from biogas: absorbent selection. RSC Adv. 3:2979–2994. doi:10.1039/c2ra23013e.

Salmi TO, Mikkola J-P, Wärnå J. 2023. Chemical reaction engineering and reactor technology. 2nd ed. Boca Raton: CRC Press.

Sanz-Perez ES, Murdock CR, Didas SA, Jones CW. 2016. Direct capture of CO_2 from ambient air. Chem Rev. 116(19):11840–11876. doi:10.1021/acs.chemrev.6b00173.

Siriwardane RV, Robinson C, Shen M, Simonyi T. 2007. Novel regenerable sodium-based sorbents for CO_2 capture at warm gas temperatures. Energy Fuels. 21:2088–2097. doi:10.1021/ef070008v.

Stolaroff JK, Keith DW, Lowry G. 2008. Carbon dioxide capture from atmospheric air using sodium hydroxide spray. Environ Sci Technol. 42(8):2728–2735. doi:10.1021/es702607w.

Wongwailikhit K. 2019. Study of gas-liquid mass transfer in bubble and spray column adding solid media [doctoral dissertation]. Bangkok: Chulalongkorn University, INSA de Toulouse; Faculty of Engineering.

Yoo M, Han SJ, Wee JH. 2013. Carbon dioxide capture capacity of sodium hydroxide aqueous solution. J Environ Manage. 114:512–519. doi:10.1016/j.jenvman.2012.10.061.

Zhang D, Deen NG, Kuipers JAM. 2007. Numerical modeling of hydrodynamics, mass transfer and chemical reaction in bubble columns. In: 6th International Conference on Multiphase Flow, ICMF 2007. [accessed 2023 Mar 23]. https://ris.utwente.nl/ws/portalfiles/portal/5529968/numerical_modeling.pdf.

Zhenqi N, Yincheng G, Wenyi L. 2009. Experimental studies on CO_2 capture in a spray scrubber using NaOH solution. In: 2009 International Conference on Energy and Environment Technology. Vol. 3. p. 52–55. doi:10.1109/ICEET.2009.479.